



Article

Blast-Induced Progressive Collapse Analysis: Accounting for Initial Conditions and Damage

Benyam Melkeneh ^{1,*}, Bedilu Habte ¹ and Girum Solomon Urgessa ²

¹ School of Civil & Environmental Engineering, Addis Ababa Institute of Technology, Addis Ababa 100, Ethiopia; bedilu@web.de

² Department of Civil, Environmental, and Infrastructure Engineering, George Mason University, Fairfax, VA 22030, USA; gurgessa@gmu.edu

* Correspondence: benyam.melkeneh@aait.edu.et

Abstract: The paper presents the progressive collapse analysis of structures, focusing on the impact of the initial conditions (particularly initial velocity) and the damage. It proposes a method that calculates the residual axial load capacity and damage of columns based on their strain profile and considers the effects of multiple blast locations. The methodology involves the conventional design of a three-story moment-resisting frame, selecting blast parameters, calculating blast pressures, and performing structural and progressive collapse analyses. The findings reveal that the Alternate Load Path Method (APM) overestimates the capacity compared to a benchmark blast–structure interaction analysis, especially when unsuitable initial conditions and damage properties are used. To address this limitation, the paper concludes the recommendations for incorporating appropriate initial conditions and damage considerations for a relatively accurate progressive collapse analysis.

Keywords: Alternate Load Path Method (APM); Single-Degree-of-Freedom (SDOF); nonlinear dynamic analysis; residual axial load carrying capacity; initial velocity; initial damage; progressive collapse



Citation: Melkeneh, B.; Habte, B.; Urgessa, G.S. Blast-Induced Progressive Collapse Analysis: Accounting for Initial Conditions and Damage. *Appl. Mech.* **2024**, *5*, 696–716. <https://doi.org/10.3390/applmech5040038>

Received: 19 August 2024

Revised: 24 September 2024

Accepted: 27 September 2024

Published: 3 October 2024



Copyright: © 2024 by the authors. Licensee MDPI, Basel, Switzerland. This article is an open access article distributed under the terms and conditions of the Creative Commons Attribution (CC BY) license (<https://creativecommons.org/licenses/by/4.0/>).

1. Introduction

Most buildings are analyzed and designed to withstand lateral forces caused by natural disasters such as earthquakes and wind. However, insufficient attention is given to the impact of man-made disasters. The amplified domestic and international security threats have elevated the likelihood of structures being exposed to blasts. Accordingly, there should be a paradigm shift in what constitutes and governs the design of new buildings and the assessment of existing buildings, especially essential buildings.

The widely used method to assess the initial local failure of structures subjected to explosions is the Direct Design Approach. This includes the Alternate Load Path Method (APM), which requires that the structure should be able to withstand the loss of a structural element without collapsing, with damage confined to the immediate area of the removed element. The idea behind the APM is to remove the column damaged by the blast load and analyze the building, if progressive collapse is imminent [1]. This means that a single column or other vertical load-bearing element is hypothetically removed without any damage to surrounding elements. This simplified approach does not accurately represent a real-world blast scenario where damage would be more dispersed and potentially affect multiple columns. It does not account for the impact of the removed element on other nearby columns that may be exposed to and damaged by the blast. Subsequently, the APM overestimates the capacity of the structure to resist collapse [2].

The objectives are to quantify: (a) the effects of non-zero initial conditions and damage to non-critical columns; (b) the assessment of structural columns for localized damage resulting from breaches, flexural failures, and direct shear failures; and (c) the progressive collapse analysis based on the removal of damaged columns, including the reduced stiffness and strength of adjacent columns, and the initial velocity.

Numerous studies have been conducted on the effect of blast load on structures especially after the destruction of the World Trade Center (WTC) [3–9]. Typical analysis commences with damage assessment of the individual vertical structural members leading to the progressive collapse analysis based on the performance levels of these members.

Shi et al. [10] proposed a new method for progressive collapse analysis by considering non-zero initial conditions. The analysis considering the removal of the ground-level column showed a redistribution of load to far-end columns leading to the absence of a trigger for progressive collapse. However, incorporating non-zero initial conditions and damage to the neighboring columns resulted in a total collapse like the benchmark analysis [10]. Gombeda et al. [11] provided an explicit threat-dependent framework for evaluating column damage. The analysis showed that significant damage to a building frame can occur even in cases where no columns are removed resulting in compromised structural integrity [11]. Based on the demand-to-capacity ratio, progressive collapse potential was assessed by Al-Salloum et al. [12]. After detonation, the column hoops ruptured, which led to loss of confinement and eventually loss of load-bearing capacity of the columns and partial collapse of the building [12]. Similar research was conducted by Kassahun [13], where an RC frame was subjected to blast load at 3 m, 5 m, 7 m and 10 m standoff distances. A critical column was removed, and nonlinear analysis was conducted to assess the potential for progressive collapse utilizing UFC guidelines [14]. Munshi [15] concluded that the realm of blast-resistant design and progressive collapse mitigation is not as extensively understood or implemented as it should be. Xu and Xiao et al. [16] showcased that initiation and propagation of progressive collapse under blast loads are often triggered by failures at beam–column connections. McConnell and Brown [17] highly stressed the ineffectiveness of the APM for small charges at the near-end and large charges at the far-end blast load. This shows the significant impact of standoff distance on behavior, and this study aims to address these limitations. Jeyarajan et al. [18] highlighted two thoughts concerning the response of the structure to a blast: the effect of strain rate and the non-conservative assessment of the APM. These findings underscore the significance of considering the column's primary role as a vertical load-bearing element, suggesting that damage criteria should be anchored in its axial capacity and overall structural behavior.

Several methods for analyzing progressive collapse in structures after explosions have limitations [3,12,17,19]. Most of the methods considered two-stage analysis, calculating the damage of columns followed by gravity load analysis for progressive collapse. However, they overlooked the initial damage and initial conditions of the columns (that is the output of the forced vibration phase)—these outputs are used as initial conditions for the free vibration phase. These initial conditions are the initial velocities and damage. This method is articulated by Shi et al. [10], who presented an improvised method for collapse analysis considering the initial damage and velocity, but this requires rigorous FEA calculation of the residual axial-load carrying capacity for individual columns. Additionally, only a single standoff distance was considered, which may not reflect real-world scenarios. Moreover, they considered only columns that completely fail during the blast, neglecting the fact that those with permanent deformation can still bear some load. Similarly, initial damage was considered by Gombeda [11], who provided a threat-dependent blast scenario that leaps ahead of APM but lacks details on how the damage translates to material degradation and in addition, zero initial conditions were considered. Methods based on the APM, like those by Al-Salloum et al. [12] and Kassahun [13], remove damaged columns without considering neighboring column damage, potentially overestimating collapse risk. Munshi [15] highlighted the importance of this topic, stating that unless there are alternative load paths with sufficient strength and ductility to redistribute the gravity load, progressive collapse is imminent. Here, the important words are 'sufficient strength and ductility' and hence, if the non-critical columns are damaged but still bear load after the blast loading, they may succumb to failure after the loss of the critical column. Therefore, deeming columns as undamaged may overpredict the potential of the building to collapse. The findings of this study outline results focused on the impact of non-zero initial velocity

and varying degrees of initial damage through stress–strain profiles of columns at different standoff distances to improve progressive collapse analysis.

The scope of the research was limited to single, relatively small charge weights that could be carried by a van. The study focused exclusively on surface or near-surface blasts and did not consider the impact of non-structural members, post-thermal loading, or ground shock.

The aim of this study is to investigate the vulnerability to progressive collapse of an idealized building subjected to blast load. This is accomplished by subjecting peripheral columns to surface blast load at different standoff distances and examining the structure under non-zero initial stress conditions, which is a realistic scenario.

The objectives of the research are the assessment of structural columns for localized damage from breach, flexural and direct shear failure, leading to either instability or global failure and the effect of non-zero initial conditions and damage of non-critical columns. If a blast can damage several columns, neighboring columns will experience comparatively lesser damage but damage, nonetheless. Subsequently, the progressive collapse analysis must be carried out based on the removal of the damaged columns (reduced stiffness and strength of the adjacent columns).

2. Material and Methods

The progressive collapse analysis was carried out in two stages: blast analysis of structural columns followed by collapse analysis based on the damage and initial conditions of these columns. The strategy followed a conventional design with blast load analysis, capacity assessment, damage assessment, and finally progressive collapse analysis, as shown in Figure 1.

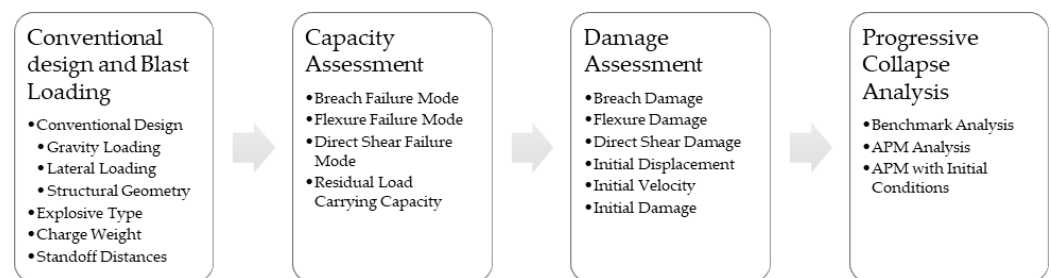


Figure 1. Research methodology.

The following concrete and rebar properties are considered for both the SDOF and LS-DYNA analyses. The characteristic cubical and cylindrical compressive strengths of concrete are 30 MPa and 25 MPa, respectively. The secant modulus of elasticity of concrete is 31 GPa, the mean axial tensile strength is 2.6 MPa, the compressive strain of concrete at peak stress is 2.1‰, the strain at maximum strength is 2.0‰, and the ultimate compressive strain is 3.5‰. Similarly, the characteristic yield strength of the reinforcement is 400 MPa, the characteristic tensile strength of the reinforcement is 600 MPa, and the characteristic strain of the reinforcement at maximum load is 20‰, while the modulus of elasticity of the rebar is 200 GPa. The steel is modeled as an elastic–plastic material with strain hardening.

2.1. Conventional Design and Blast Loading

The blast load (charge weight) considered was 345 kg ANFO (300 kg equivalent TNT). The standoff distance of the blast was separated into a rectangular array, as shown in Figure 2. The nearest location was placed 4 m from the face of the perimeter column and divided in plan by 1.5 m grid spacing parallel to the depth of the building up to 8.5 m and by 3 m throughout the width of the building, totaling 12 blast locations (without considering symmetry). The first three blasts were detonated at a height of 0.5 m above the ground to mimic vehicle-borne loading and to induce direct shear failure, and the remaining detonations occurred at height of 1.5 m above the ground floor to induce flexural

failure. Figure 3 shows the locations for calculating the response and pressure of columns. Odd points are used for computing direct shear and breach, while even points are used for assessing flexure.

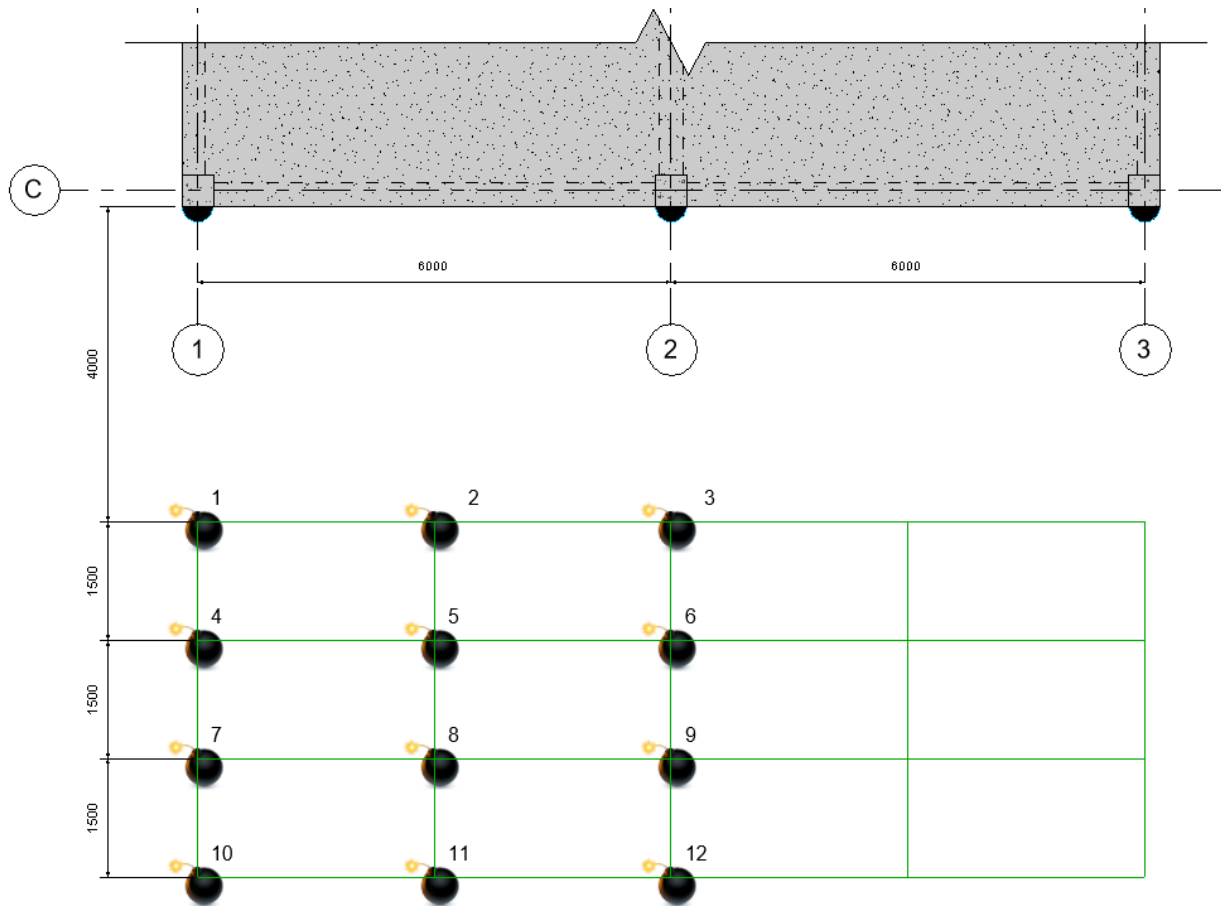


Figure 2. Blast locations.

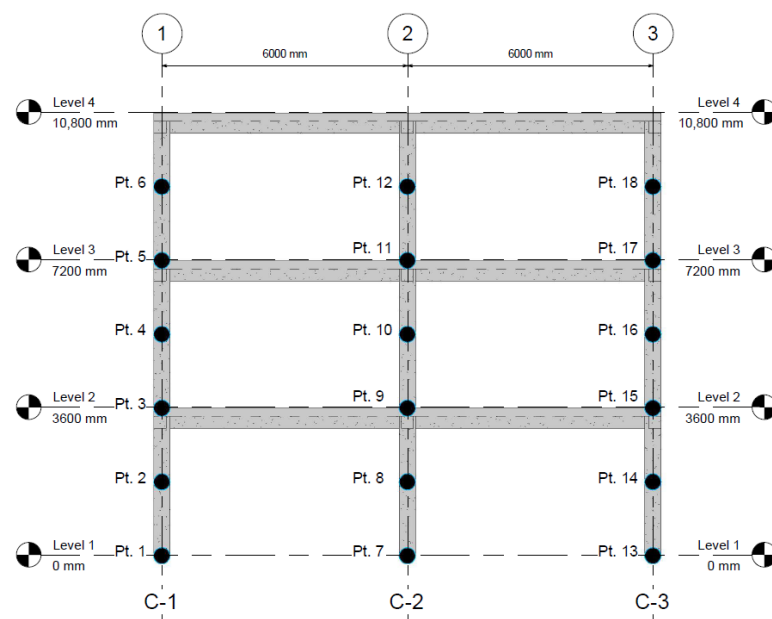


Figure 3. Column pressure positions.

The conventional design followed the following standard codes: EN 1990 [20], EN 1991-1-4 [21], EN 1992-1-1 [22] and EN 1998-1-1 [23]. The gravity load parameters considered are the total dead load including partition (excluding self-weight) was 4.5 kN/m^2 and the total live load was 3 kN/m^2 for all floors. The wind load parameters are basic wind speed of 35 m/s , terrain category IV, and air density of 0.94 kg/m^3 . The seismic load parameters are the peak ground acceleration of 0.1 g , spectrum type 1, ground type B, and behavior factor of 3.9. Finally, global imperfection is considered with a basic value of inclination of $1/200$.

2.2. SDOF Assessment of Columns

Assuming damage in beams is preserved by the rigid floor diaphragm, capacity assessment is conducted for the columns. The dynamic properties of reinforced concrete under high strain rates were first investigated, including both concrete and rebar. This is expressed through the dynamic increase factor (DIF), defined as the ratio of the material's dynamic strength (measured under blast loading) to its static strength (obtained under slow, controlled loading) at a particular strain rate. The DIF is calculated based on the tabulated data presented in UFC [14].

Breach failure mode was calculated using the empirical formula presented in Blast Effects on Buildings [24]. On the contrary, flexure and shear failure modes were calculated using SDOF. The modeling of columns in continuous frames typically involves the selection of appropriate boundary conditions, with the three most common options being fixed–fixed (both ends rigidly restrained against rotation and translation), fixed–simple (one end fixed and the other allowed to rotate but not translate), and simple–simple (both ends allowed to rotate and translate). Here, fixed–fixed boundary condition is utilized. The SDOF analysis followed a fixed-end column with a uniformly distributed load as it depicts the building under study. The initial conditions used to solve the second-order differential equations of the SDOF are zero initial displacement and velocity.

2.2.1. Breach Failure Mode

The significant concentrated pressure necessary to breach a reinforced concrete element result in this failure mode and is frequently associated with the intense demands of close-in explosions.

2.2.2. Flexure Failure Mode

Flexural performance evaluation employs standardized resistance functions defined in DoD [1] and a simplified SDOF analysis framework. Each column was represented as a mass-spring system with a single translational degree of freedom in the horizontal direction parallel to the exciting force. The equation of motion incorporating axial load, as presented by Liu et al. [25], is shown in Equation (1) and Figure 4. Here, k denotes the system's resistance as a function of displacement x , M represents the equivalent mass, $P(t)$ denotes the reflective pressure load over time, K_{LM} is the transformation factor, c is the damping coefficient and P_a represents the axial load.

$$K_{LM}M\ddot{x} + c\dot{x} + kx = P(t) + 8\frac{P_a}{L}x \quad (1)$$

The axial load represents the static load, according to GSA [26] guidelines represented by a dead load plus 25% of the live load. The resistance function followed three stages: elastic, elastoplastic, and plastic. The elastic stage is where the concrete retains its tensile strength. The elastoplastic stage follows the elastic stage until the reinforcement reaches its yield strength. Finally, at the plastic stage, plastic hinges are formed at the mid-span when the ultimate deflection is reached. Solving a nonlinear system using this trilinear resistance function results in an unrealistic response or numerical error. Therefore, the trilinear resistance function is converted to a bilinear resistance curve, as proposed by Carvalho [6].

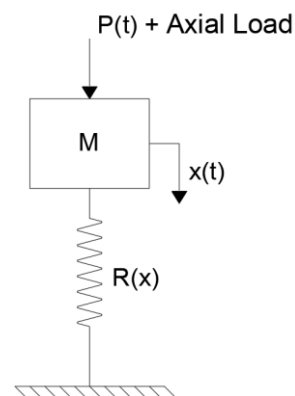


Figure 4. Equivalent SDOF including axial load.

The contribution of structural damping to overall energy dissipation is minimal compared to plastic deformations [27]. Nevertheless, damping was incorporated and the damping coefficient (c) is calculated using a damping ratio of 5% based on the recommendations of Kyei [28].

2.2.3. Direct Shear Failure Mode

Direct shear resistance of columns is attributed to their initial dynamic rigid body motion, observed before the onset of flexural response. This rigid body behavior results in a localized concentration of shear stresses near the supports. Accurately modeling the direct shear resistance of RC structures remains a challenge, leading to a reliance on empirical approaches. The resistance–slip model, pioneered by Krauthammer et al. [29], represents a significant step in this direction. Like the flexural resistance, the shear resistance is converted to a bilinear model using the energy balance method proposed by Cui et al. [30]. Considering the two supports and axial load (increases shear resistance), a revised shear resistance given by Gombeda et al. [11] was utilized for conducting the direct shear resistance.

2.2.4. Residual Axial Load Carrying Capacity

The residual axial load carrying capacity is the initial damage a column absorbs after the blast duration. This initial damage entails whether the damaged column can sustain a certain degree of load-carrying capacity. A rigorous method was proposed by Shi et al. [31]. This research, however, followed another simplified method for calculating the residual axial-load carrying capacity based on the stress–strain profile of each column. A more practical method, based on mechanics for RC bridge columns, as proposed by Warn and Unal [32].

The residual axial capacity is a combination of the resistances of the concrete and rebar. The concrete carrying capacity is determined by calculating the curvature at maximum drift (sum of the yield and plastic curvature which are functions of the concrete depth and end rotations). Based on this curvature, the maximum strain in the compressive zone of the concrete is obtained. Comparing this to the maximum strain the concrete can carry before failure, the crushing depth is determined. Therefore, the residual axial load-carrying capacity of the concrete is a function of the uncrushed net area of concrete (without reinforcement) and the compressive strength. Once the axial load carrying capacity of the concrete is calculated the axial load capacity of the reinforcement is followed. This is based on the minimum capacity of either the plastic resistance or buckling resistance. In both cases, the reinforcement is treated as a beam spanning between two transverse reinforcements. Hence, the total axial load-carrying capacity is the sum of both the concrete and rebar.

The damage degree, as provided by Shi et al. [31], is a function of the ratio of the residual axial load-carrying capacity to the nominal one, specified in ACI 318-19 [33].

2.3. Damage Assessment

The evaluation of the flexural limit states of the columns employed response criteria established by U.S. Army Corps of Engineers [34]. The damage levels were constrained by four response limits presented by ASCE/SEI-11 [35] with the corresponding description of the damage presented by U.S. Army Corps of Engineers [34].

The shear response limits were defined by limiting the shear strain considering the shear slip [30]. Like the flexural response, SDOF analysis is computed for evaluating shear slip using the proposed resistance function.

The damage degree was translated in the model through material strength and stiffness degradation, as proposed by Shi et al. [10].

2.4. Finite Element Analysis with LS-DYNA

The finite element analysis was conducted using LS-DYNA. There are three methods in LS-DYNA to account for blast loading on structures [36]: 'Load_Blast_Enhanced', Arbitrary Lagrangian-Eulerian (ALE), and direct pressure–time history. In this research, 'Load_Blast_Enhanced' is considered as it provides a more practical solution for resource-limited scenarios, compared to the ALE method and experimental data.

The best-suited concrete constitutive model for this research was Mat_Concrete_Damage_REL3. To account for failure of concrete, an erosion method was applied to remove certain elements of the concrete material after failure. The failure criteria considered were principal strain and shear strain. When the plastic strain exceeds 15% and/or the shear strain exceeds 90%, the concrete element is eroded. These values were concluded after replicating the experiment conducted by Zhang et al. [37] and Siba [9]. Moreover, the same erosion thresholds were used by Shi et al. [10], and Tantrapongsaton et al. [38]. It is important to note that the erosion technique is a numerical tool used to address excessive mesh distortion in simulations [10]. Erosion represents various physical phenomena leading to material loss or discontinuity, such as shear, cratering, spalling, and fracture. MAT_PIECEWISE_LINEAR_PLASTICITY was selected as the beam element as it allows for defining arbitrary stress–strain curves.

2.5. Progressive Collapse Analysis

Three analyses were carried out for each blast location: the APM method, the APM plus initial condition, and the blast–structure interaction. Based on these methods the potential for collapse was assessed. The most important outputs were vertical and transverse displacement, and vertical velocity. Vertical displacement dictates the displacement–time history under gravity loading; the lateral displacement shows the transverse displacement parallel to the blast load; and the vertical velocity indicates the rate of collapse.

The initial conditions (velocity) for the non-critical columns obtained from SDOF analysis were assigned as a preload for progressive collapse analysis. The results of the three analyses were used to determine whether total collapse or partial collapse occurs, and the respective values of the output (vertical displacement, transverse (Y-direction) displacement and vertical velocity) were compared. The nodal location for computing the responses was on axis C-2 at the 1st-story level.

3. Results

Based on the conventional design, the selected perimeter columns were 400 mm × 400 mm with 8#16 bars and the critical region confinement stirrup was diameter 8 with a center-to-center spacing of 120 mm. Similarly, the interior column has dimensions of 500 mm × 500 mm, the floor beams have dimensions of 500 mm × 300 mm (Depth × Width), and the slab has a thickness of 200 mm. All the beams are reinforced with 4#20 continuous bottom bars and 2#20 continuous top bars, along with 3#20 additional top bars. All the slabs are reinforced with #10 bars spaced 200 mm center-to-center for the bottom reinforcement and #10 bars spaced 120 mm center-to-center for the top reinforcement, except at the ends, where the spacing is 200 mm.

The reflected pressure–time history, considering peak overpressure, positive time duration, time of arrival and wave decay parameter, were obtained based on Kingery–Bulmash equations. Figure 5 shows the reflected pressures for blast detonations at 1, 3 and 6 with points indicating the locations in columns specified in Figure 3.

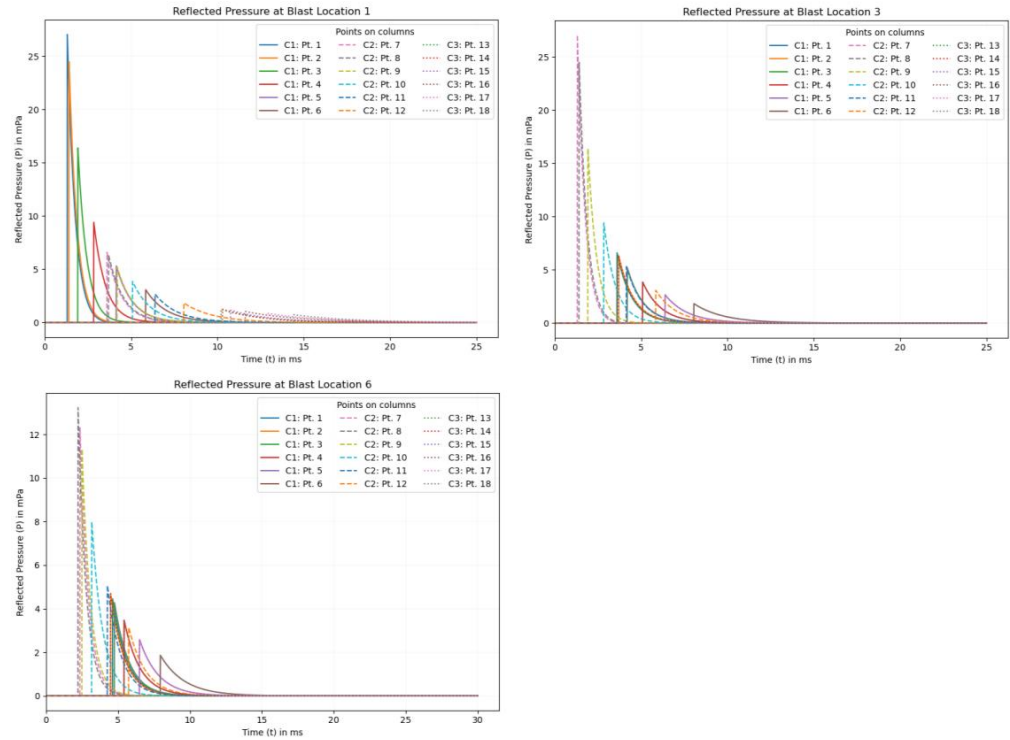


Figure 5. Reflected pressures at blast locations 1, 3, and 6.

3.1. Capacity Assessment of Columns

Based on the empirical formula presented by Cormie et al. [24], none of the columns at any story level and standoff distance were exposed to breach. The minimum depth of a column that would result in a breach was determined to be 84 mm.

The flexural response is computed by solving the nonlinear dynamic analysis using Newmark’s Beta method (average acceleration), as described by Chopra [39]. Figures 6–8 show the mid-span deflections and velocity histories of columns at the specified blast locations. Similarly, Figures 9–11 show the shear slip histories at the column ends.

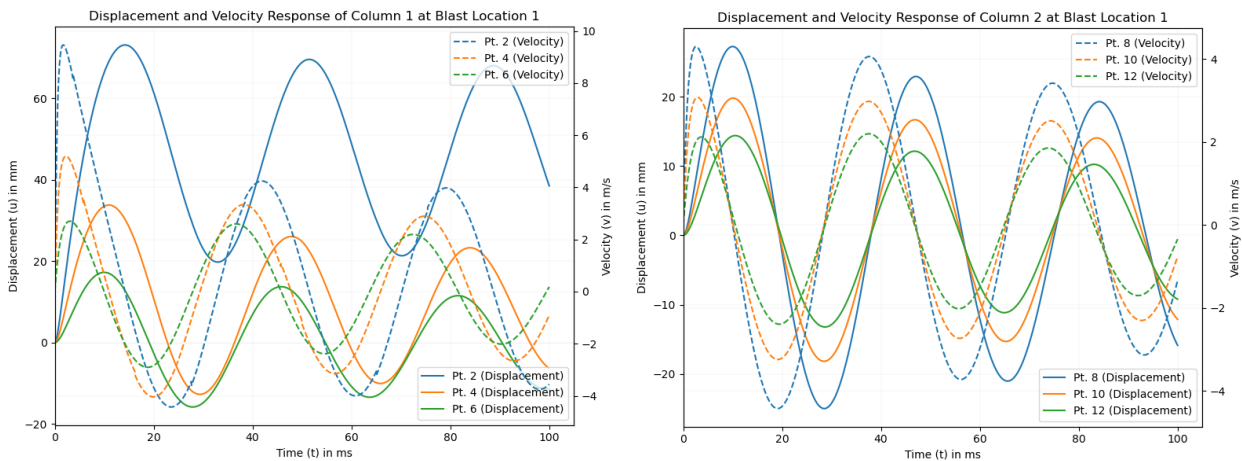


Figure 6. Displacement and velocity histories of columns 1 and 2 at blast location 1.

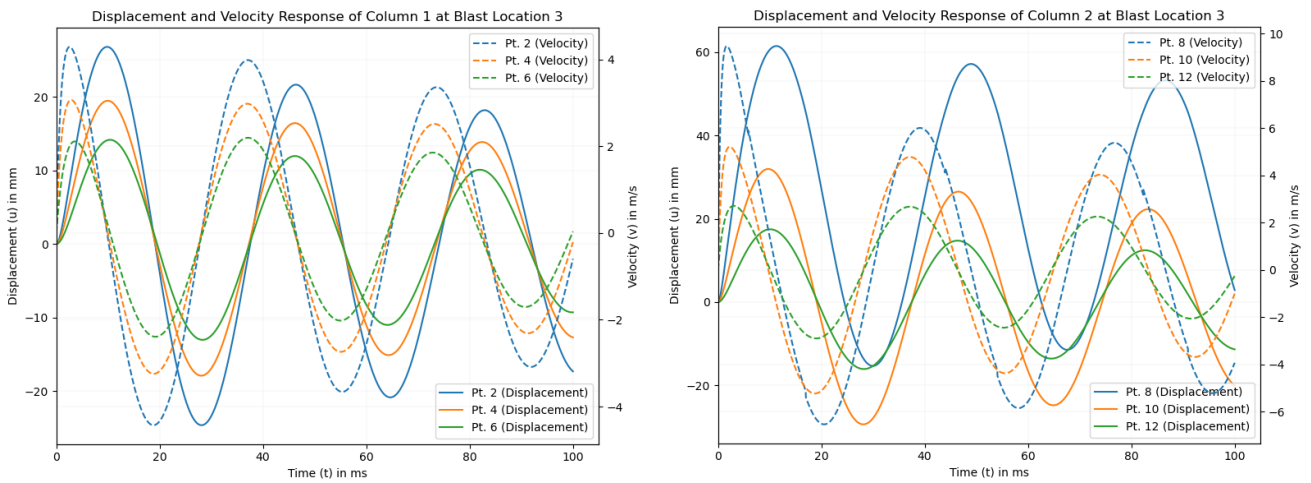


Figure 7. Displacement and velocity histories of columns 1 and 2 at blast location 3 (column 3 at points 14, 16 and 18 (similar to column 1)).

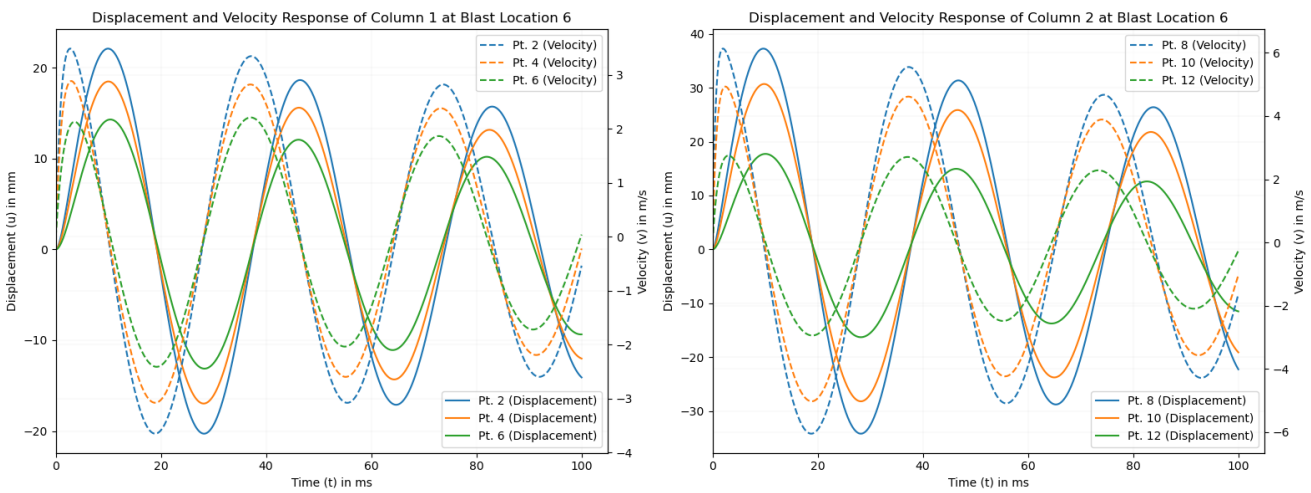


Figure 8. Displacement and velocity histories of columns 1 and 2 at blast location 6 (column 3 at points 14, 16 and 18 (similar to column 1)).

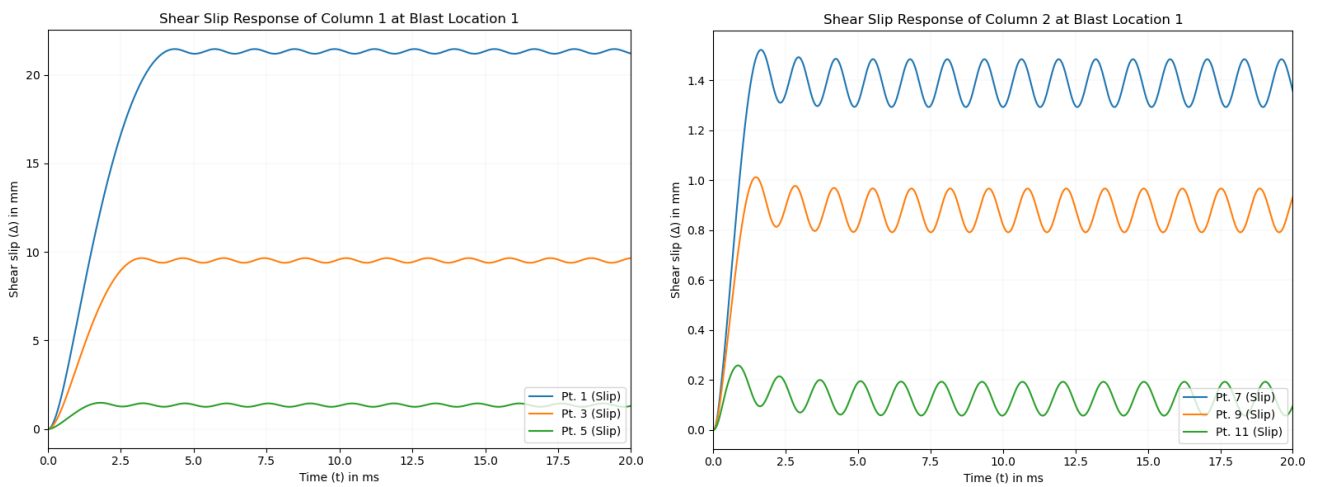


Figure 9. Direct shear responses of columns 1 and 2 at blast location 1.

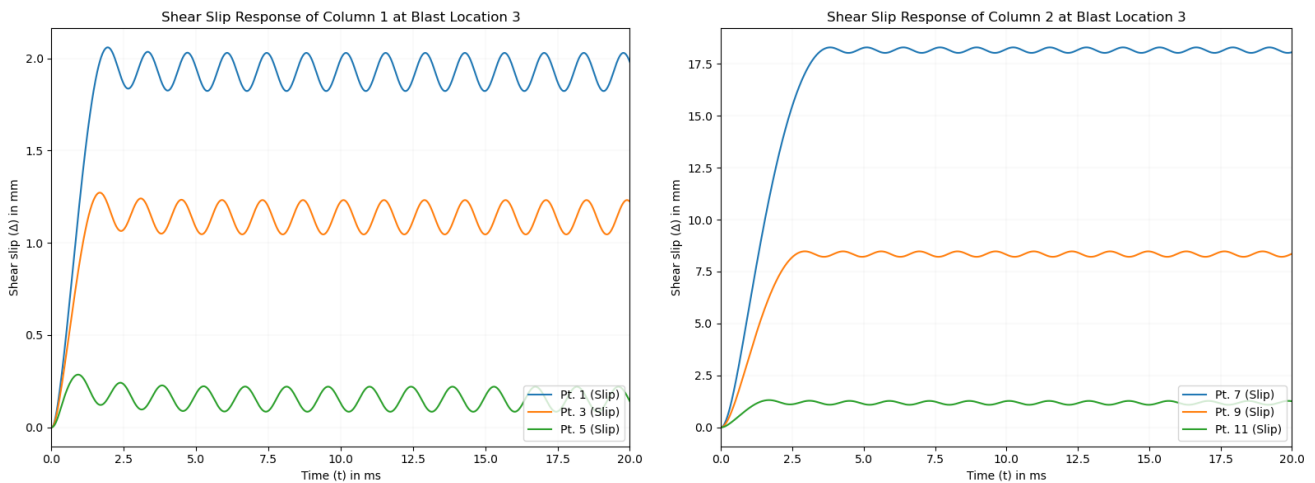


Figure 10. Direct shear responses of columns 1 and 2 at blast location 3 (column 3 at points 13, 15 and 17 (similar to column 1)).

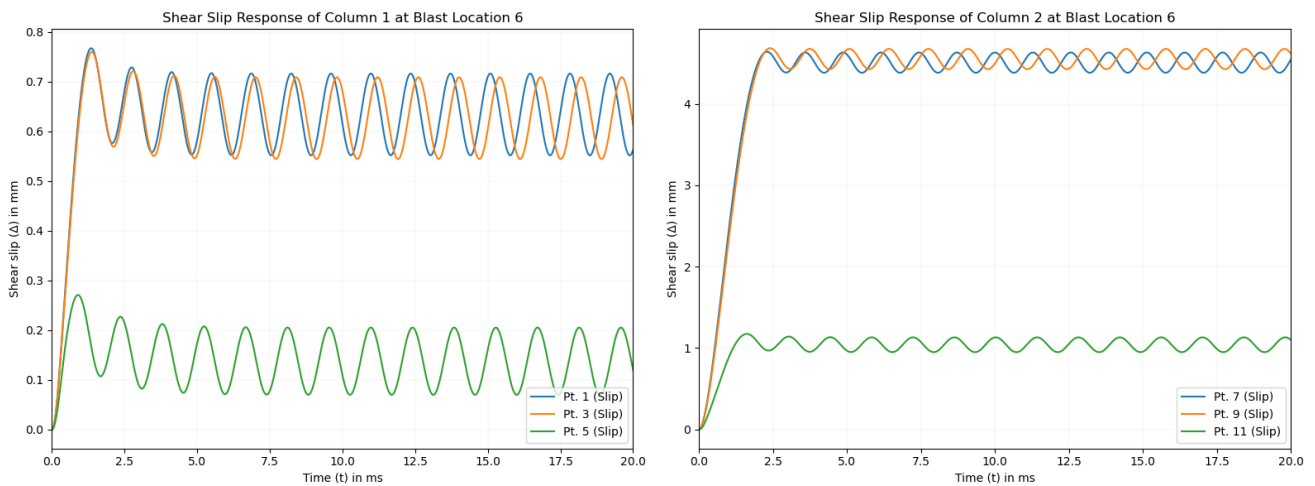


Figure 11. Direct shear responses of column 1 and 2 at blast location 6 (column 3 at points 13, 15 and 17 (similar to column 1)).

3.2. Validation of SDOF System

Two different experimental results from two different sources were considered: Zhang et al. [37] and Siba [9]. Zhang et al.’s experiment involved a spherical air burst on a beam with dimensions of 100 mm × 100 mm × 1100 mm. The standoff distance was fixed at 0.4 m and the charge weight was varied. The prevailing failure mode was flexural with scabbing of the covers at a higher charge weight. The scaled distance varied from 0.57 to 0.40 m/kg^{1/3}. Figure 12 shows the mid-span displacement histories for beams B2-1 to B2-4.

As shown in Table 1, the SDOF gave a reliable result regarding the response of the structure especially at higher charge weights. There is no universally accepted margin of error between experimental and numerical results in engineering. However, several resources discuss common practices and considerations [30,40]. According to Timsah et al. [40], the maximum allowed margin of error is 9.25% and, as per Cui et al. [30], the accepted margin of error varies from −11.2% to 58.3%. The calculated errors in this research vary from 34.22% (for sample B2-1, which showed an increase in displacement of only 3 mm) to 3.58% and hence, the SDOF is regarded as acceptable for practical uses. More significantly, the prevailing failure mode, flexural failure, was well represented as indicated by the ductility ratio and rotation.

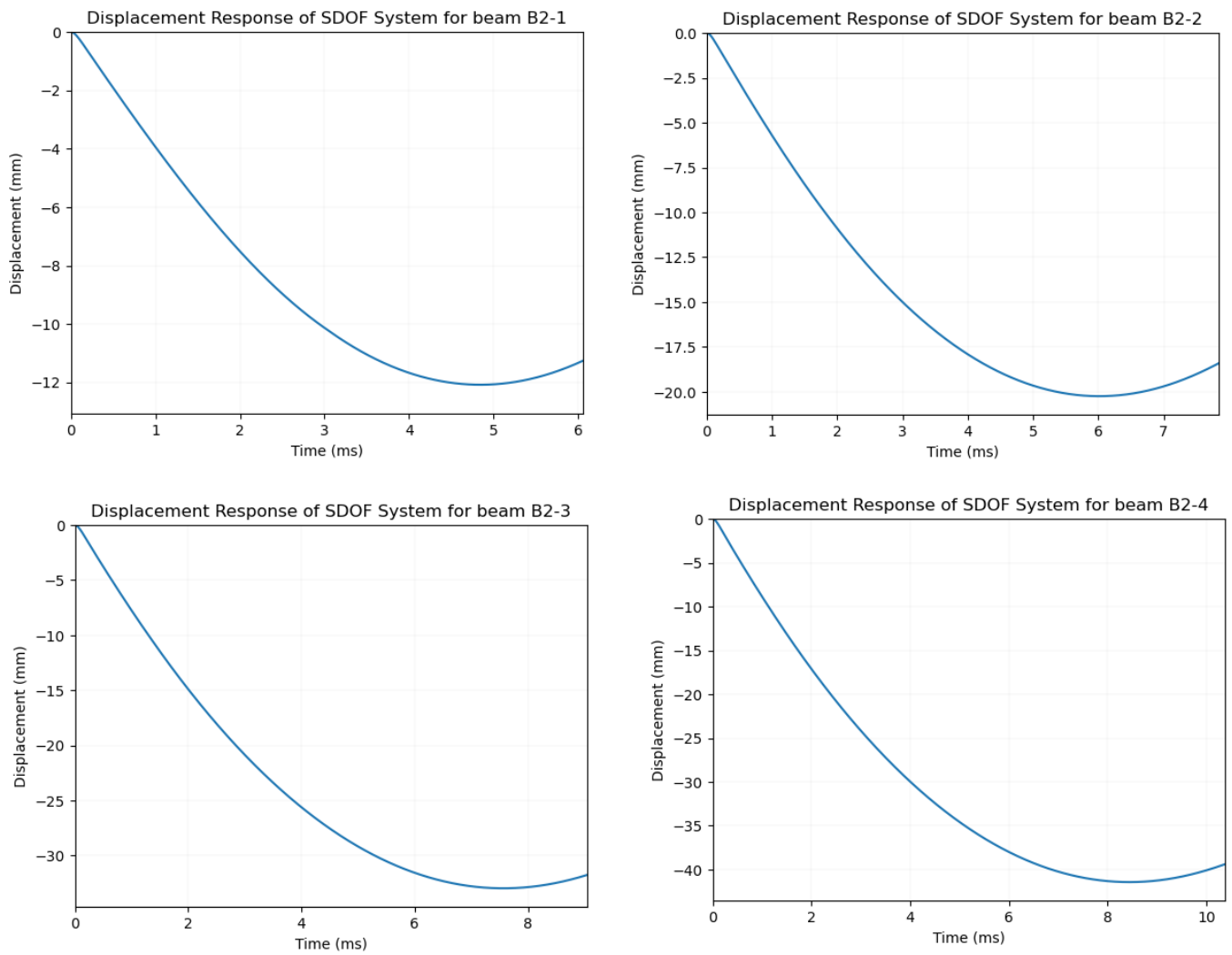


Figure 12. Flexural responses for beams B2-1 to B2-4 of Zhang et al.’s experiment.

Table 1. Comparison of the test and SDOF results.

Beam	Scaled Distance (m/kg ^{1/3})	Test Central Deflection (mm)	Flexure		Direct Shear	
			Δ_{max} (mm)	Error (%)	Δ_{max} (mm)	γ (%)
B2-1	0.57	9	12.08	34.22	0.39	0.45
B2-2	0.50	25	20.25	−19.00	0.68	0.78
B2-3	0.44	35	33.00	−5.71	1.22	1.41
B2-4	0.40	40	41.43	3.58	1.59	1.84

For additional validation, Siba’s experiment, with shear as the prevailing failure mode in addition to some flexural cracks, is considered. The column has dimensions of 300 mm × 300 mm × 3000 mm subjected to charge weights of 82 kg and 123 kg TNT equivalent of ANFO at different standoff distances. Most of the gauges were deemed unreliable due to damage but the SDOF analysis showed that shear is the prevailing failure mode (Figure 13) with a maximum shear slip of 12.4 mm and an average shear strain of 4.77%.

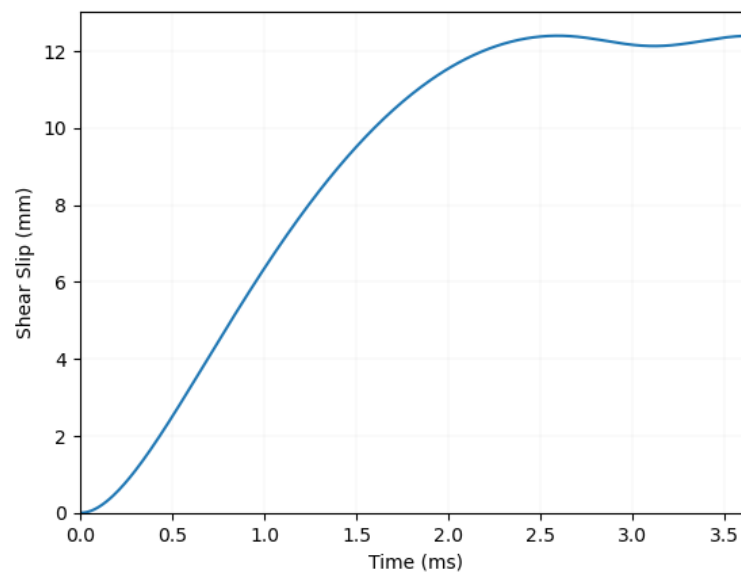


Figure 13. Shear response for RC column of Farouk’s experiment.

3.3. Building’s Vertical Elements Response

For this research, the responses (flexural and direct shear) for each column based on the selected charge weight and standoff distance are shown in Figures 6–11 and Table 2. The selected standoff distances that resulted in progressive collapse are blast locations 1, 3 and 6.

Table 2. Flexure, direct shear and damage response levels of the building columns.

Blast Location	Column	Point	Flexure							Point	Direct Shear		
			Maximum Displacement (mm)	Ductility Ratio	Rotation (Degree)	Damage Degree	Velocity (m/s)	Response Level	Component Damage		Maximum Shear Slip (mm)	Average Shear Strain (%)	Component Damage
1	Axis 1-C	2	73.15	3.03	2.70	0.252	9.46	B4	Hazardous Damage	1	21.45	6.20	Severe Damage
		4	33.80	1.69	1.25	0.198	5.20	B3	Heavy Damage	3	9.65	2.79	Moderate Damage
		6	17.25	1.12	0.64	0.123	2.70	B3	Heavy Damage	5	1.48	0.43	Minor Damage
	Axis 2-C	7	27.24	0.74	1.01	0.000	4.30	B1	Superficial Damage	7	1.52	0.44	Minor Damage
		10	19.79	0.68	0.73	0.000	3.07	B1	Superficial Damage	9	1.01	0.29	Minor Damage
		12	14.39	0.70	0.53	0.000	2.20	B1	Superficial Damage	11	0.26	0.07	Minor Damage
	Axis 3-C	14	12.42	0.51	0.46	0.000	1.88	B1	Superficial Damage	13	0.10	0.03	Minor Damage
		16	22.48	1.13	0.83	0.000	2.72	B3	Heavy Damage	15	0.10	0.03	Minor Damage
		18	16.80	1.09	0.62	0.000	2.01	B3	Heavy Damage	18	0.09	0.02	Minor Damage
3	Axis 1&3-C	2, 14	26.84	1.11	0.99	0.175	4.29	B3	Heavy Damage	1, 13	2.06	0.59	Minor Damage
		4, 16	19.50	0.98	0.72	0.000	3.07	B2	Moderate Damage	3, 15	1.27	0.37	Minor Damage
		6, 18	14.19	0.92	0.52	0.000	2.20	B2	Moderate Damage	5, 17	0.29	0.08	Minor Damage
	Axis 2-C	7	61.47	1.66	2.27	0.243	9.47	B3	Heavy Damage	7	18.29	5.28	Severe Damage
		10	31.96	1.10	1.18	0.192	5.21	B3	Heavy Damage	9	8.47	2.45	Moderate Damage
		12	17.49	0.85	0.65	0.000	2.71	B1	Superficial Damage	11	1.31	0.38	Minor Damage
6	Axis 1&3-C	2, 14	22.10	0.91	0.82	0.000	3.49	B2	Moderate Damage	1, 13	0.77	0.22	Minor Damage
		4, 16	18.48	0.93	0.68	0.000	2.89	B2	Moderate Damage	3, 15	0.76	0.22	Minor Damage
		6, 18	14.30	0.93	0.53	0.000	2.21	B2	Moderate Damage	5, 17	0.27	0.08	Minor Damage
	Axis 2-C	7	37.25	1.01	1.38	0.206	6.14	B3	Heavy Damage	7	4.64	1.34	Minor Damage
		10	30.69	1.05	1.13	0.189	4.93	B3	Heavy Damage	9	4.68	1.35	Minor Damage
		12	17.73	0.87	0.66	0.000	2.75	B1	Superficial Damage	11	1.17	0.34	Minor Damage

3.4. Finite Element Analysis Validation

The finite element analysis results were compared with the experimental results from Zhang et al. [37]. Figure 14 presents the displacement-time history of beam B2-4 as obtained from LS-DYNA.

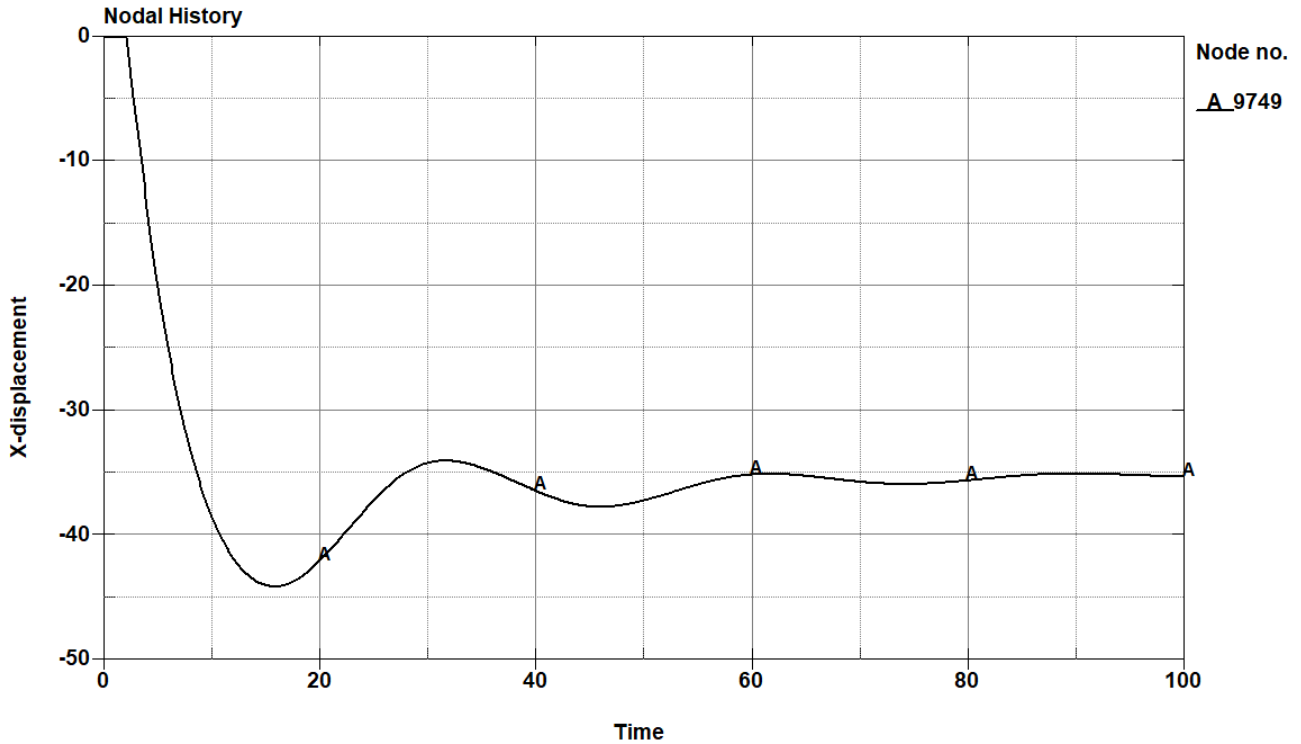


Figure 14. Displacement history of Zhang et al. experiment in LS-DYNA.

B2-4 was selected to showcase both the response and the scabbing of the concrete cover. The maximum displacement of the experiment was 40 mm whereas the maximum displacement according to LS-DYNA was 44.1 mm, and 41.43 mm from SDOF. Consequently, the margins of errors are 10.25% and 6.05% compared to the experimental value and the SDOF analysis, respectively. The faces of beam B2-4 at the end of loading are shown in Figure 15. This demonstrates that the erosion method and the values of principal and shear strain considered are justified. This is further corroborated by replicating the experiment conducted by Farouk, as shown in Figure 16.

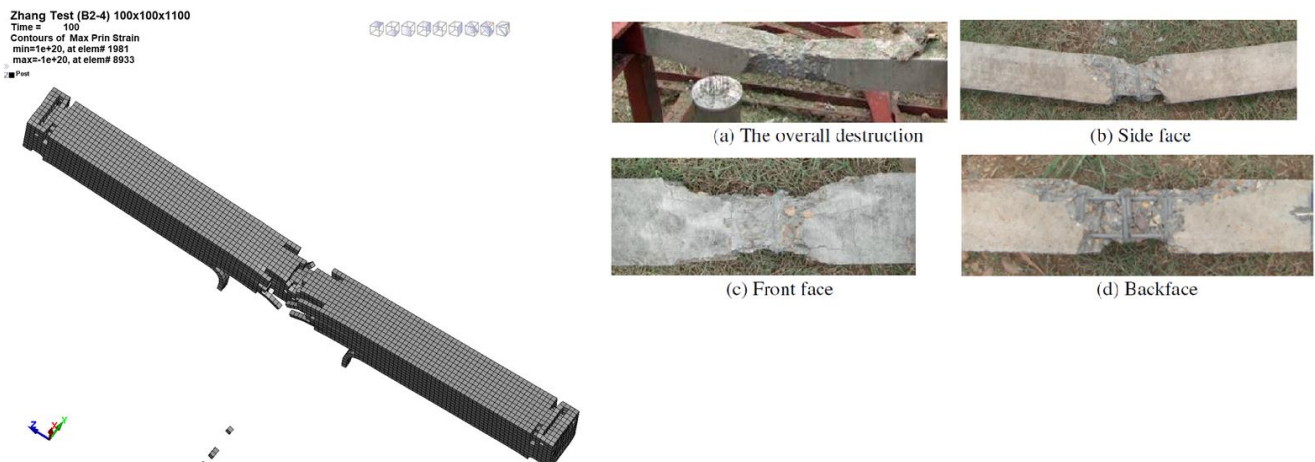


Figure 15. Deflection of beam B2-4 in LS-DYNA and Zhang et al. experimental damage [32].

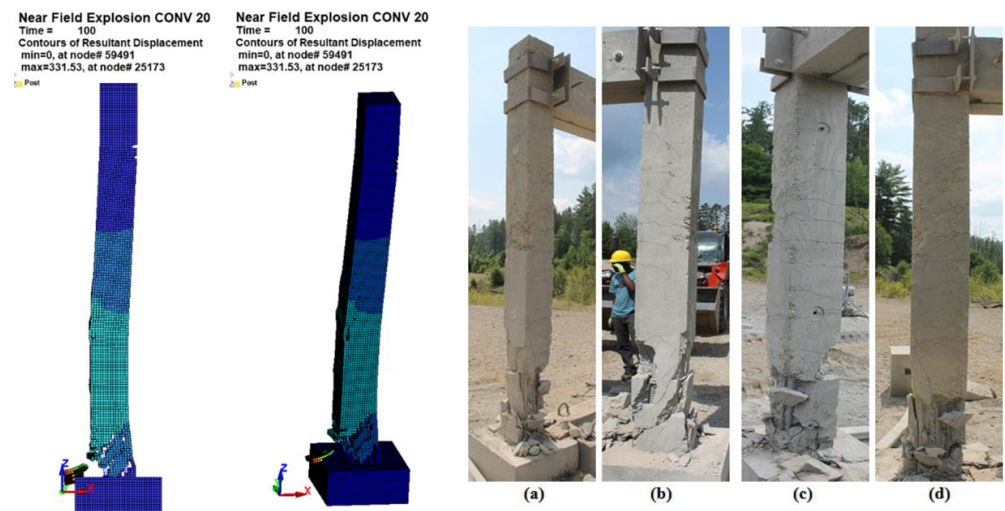


Figure 16. Side face and isometric view deflection of Farouk’s column in LS-DYNA and Farouk’s Column damage (Conv20): (a) front face; (b) side face (right); (c) back face; and (d) side face (left) [9].

3.5. Collapse Analysis

Under blast location 1, according to the Blast_Enhanced method, the progressive collapse begins by direct shear failure of first-story column on axis 1, followed by plastic hinge formation at the ends of first-story beams on axis C (1–2), accompanied by failure of the column on axis 2, and finally formation of plastic hinges at the ends of the first-story beams on axis C (2–3) and the pullout of this beam from axis C-3. Partial collapse was observed between axes B–C and 1–3.

Based on the APM with initial conditions, the first-story column on axis 1 was removed before collapse analysis. A similar collapse pattern is observed under the APM with initial conditions. However, based on the APM method, collapse begins with the formation of plastic hinges at the first-story beams on axes B and C, but this terminates at the first-story column on axis 2. Subsequently, a partial collapse was observed on grids 1–2 and B–C only, as shown in Figure 17, whereas, under the APM with initial conditions and Blast_Enhanced methods, a partial collapse was observed on grids 1–3 and B–C, as shown in Figure 17. Figure 18 shows the nodal vertical displacement and indicates that the first-story column on axis 2 under the APM method remains load bearing, unlike in the APM with initial conditions and the Blast_Enhanced method. Figures 18–20 show the nodal lateral displacement and vertical velocity, respectively. The time gap between the APM with initial conditions and the Blast_Enhanced method was dependent on the time it takes for the first-story column on axis 1 to reach failure (unable to bear load) and the arrival time of blast loading and in contrast, the APM with initial conditions commences with an already removed column.

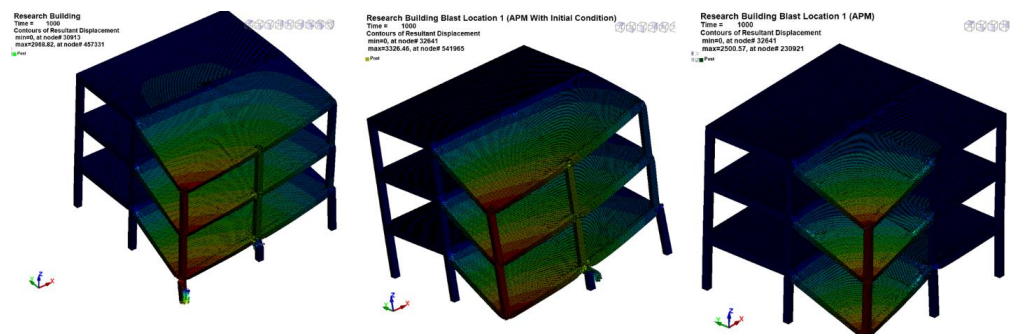


Figure 17. Blast_Enhanced, APM with initial conditions and APM method of analysis at partial collapse (blast location 1).

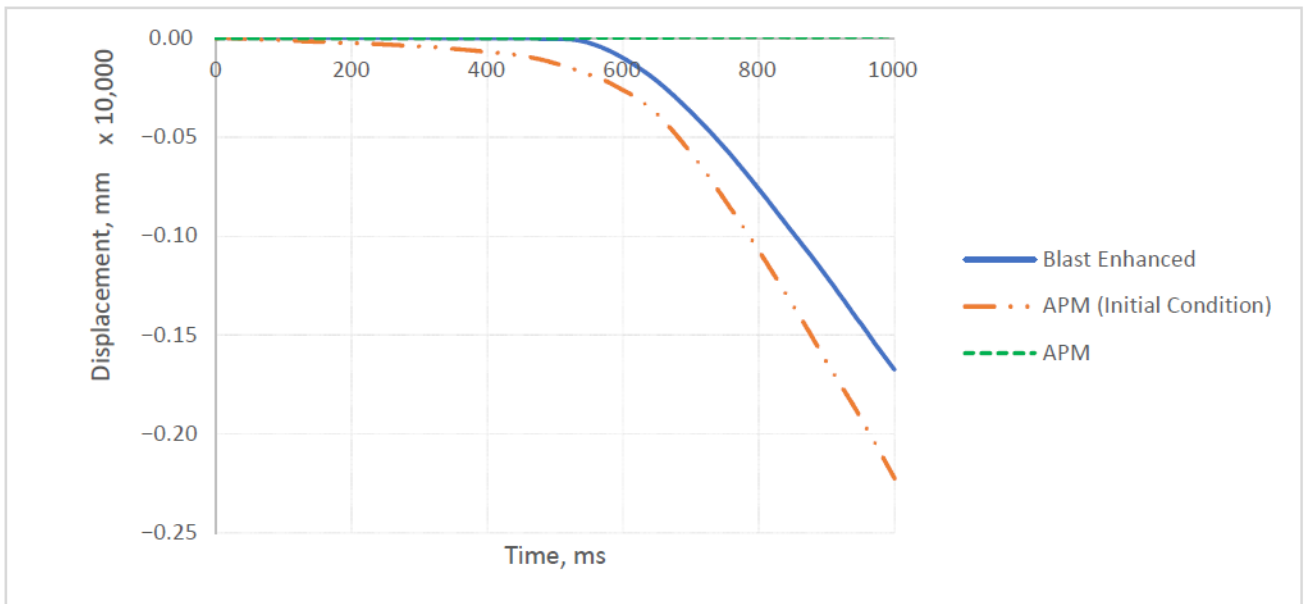


Figure 18. Nodal vertical displacement comparison at blast location 1.

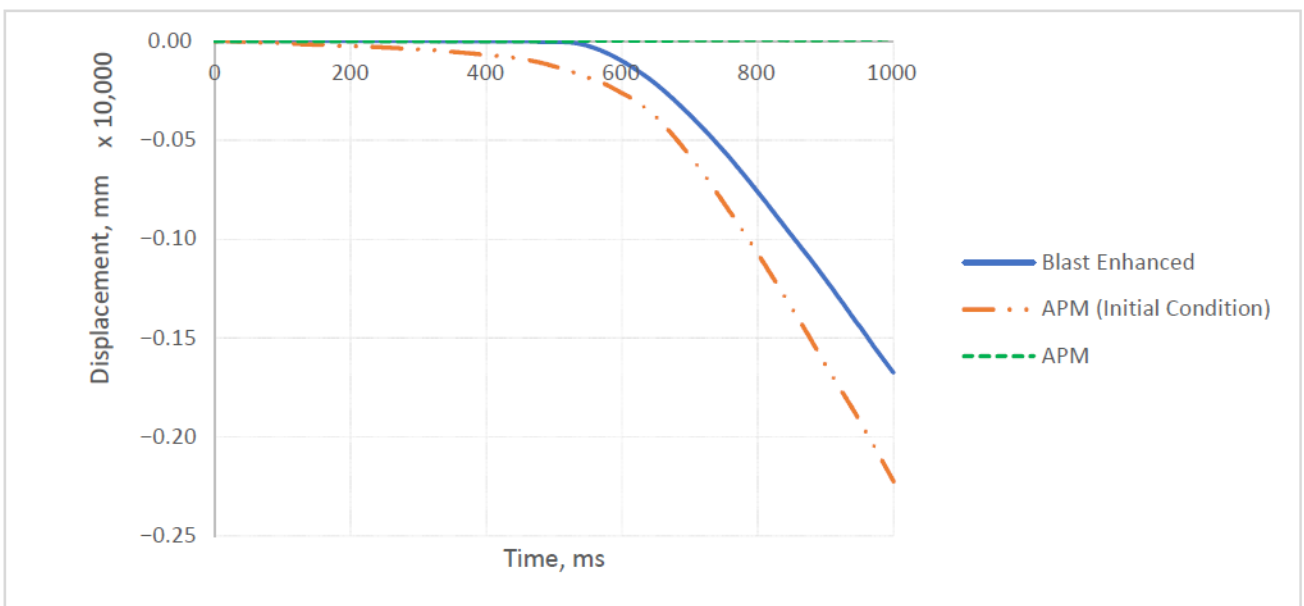


Figure 19. Nodal lateral displacement (Y-direction) comparison at blast location 1.

At blast location 3, the column on axis C-2 failed by direct shear, and that was confirmed by both SDOF and LS-DYNA analyses. Based on the Blast_Enhanced method of analysis, the column on axis C-2 failed first due to direct blast loading, followed by plastic hinge formation on axes C-1 and C-3 caused by the distribution of load to the neighboring columns above the first floor. Finally, these joints were pulled out of the beam–column connection, resulting in the partial collapse of the structure from axes B-1 and B-3 to C-1 and C-3. Similar trends in failure and response were obtained by both the APM and the APM with initial conditions, as shown in Figures 21–24. Similar results were observed across all methods of analysis due to the removal or failure of a highly stressed column, as demonstrated by Abebe et al. [41] in their study of progressive collapse in both typical and atypical reinforced concrete framed buildings.

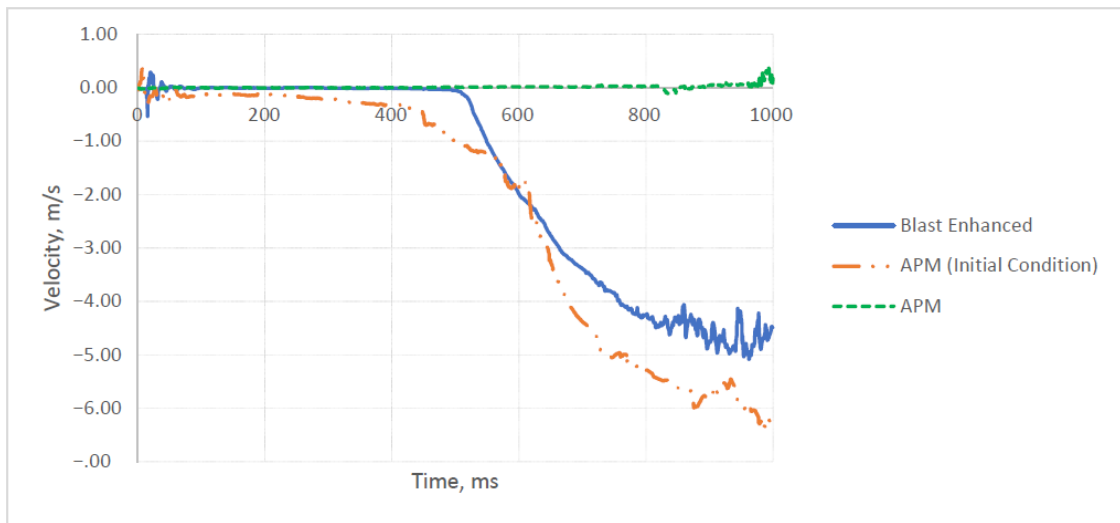


Figure 20. Nodal vertical velocity comparison at blast location 1.

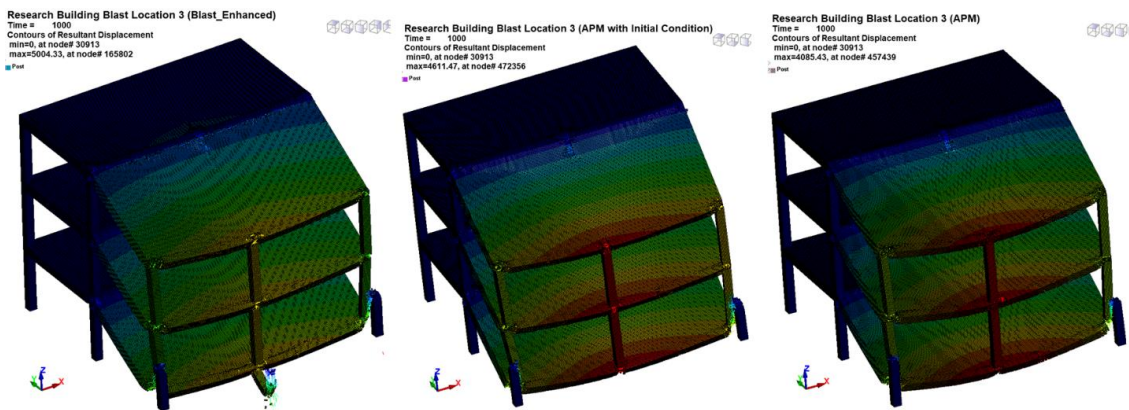


Figure 21. Blast_Enhanced, APM with initial conditions, APM method of analysis at partial collapse (blast location 3).

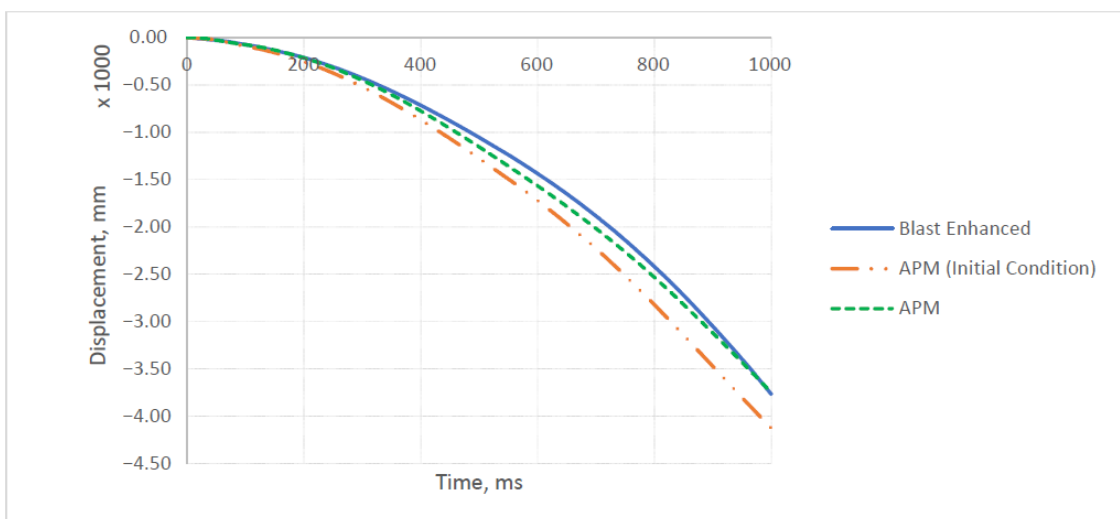


Figure 22. Nodal vertical displacement comparison at blast location 3.

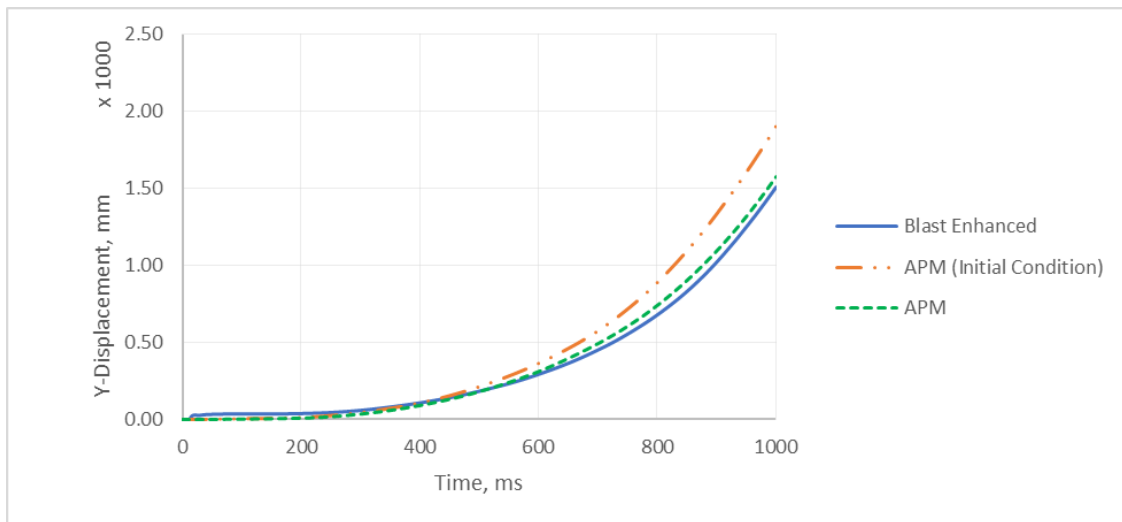


Figure 23. Nodal lateral displacement (Y-direction) comparison at blast location 3.

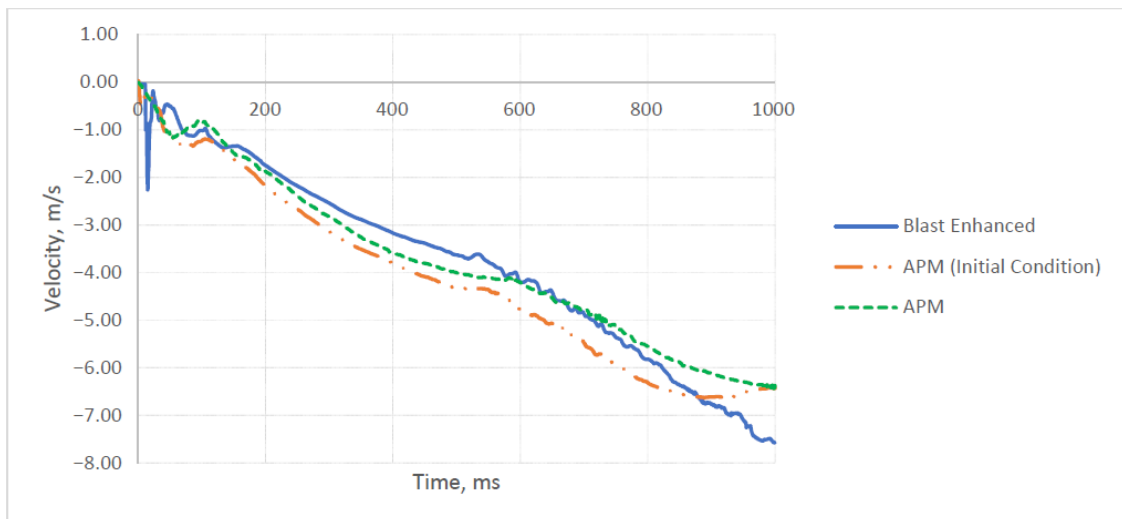


Figure 24. Nodal vertical velocity comparison at blast location 3.

The main differentiating aspect between the APM and both the Blast_Enhanced and the APM with initial conditions is the response where none of the columns fail under direct blast loading. This was clearly seen with blast location 6. Under the Blast_Enhanced method, at blast location 6, the first-story column on axis C2 under direct blast loading was exposed to permanent deflection, as shown in Table 2, but it remains a load-bearing member. After the blast loading duration, this column experienced a large deflection leading to failure. Like blast location 3, due to the failure of the column on axis 2, columns 1 and 3 were subjected to large axial loads and moments and subsequently, failure of these columns was triggered. Before the failure of column 2, multiple plastic hinges appeared at axes 1, 2 and 3. Likewise, according to the APM with initial conditions, a similar failure was obtained. However, the duration of failure of the column on axis C-2 is longer, as shown in Figure 25, and the failure mechanism compared to the Blast_Enhanced method was different. The column failed at the mid-span and at the beam-column joint for the Blast_Enhanced method and the APM with initial conditions, respectively, as shown in Figure 26. As shown in Figure 27, the lateral displacement between the two methods increases as time progresses. Nevertheless, after 1250 ms, the initiation of progressive collapse on axes B-C and 1-3 commenced following the formation of multiple plastic hinges at grid C from 1 to 3.

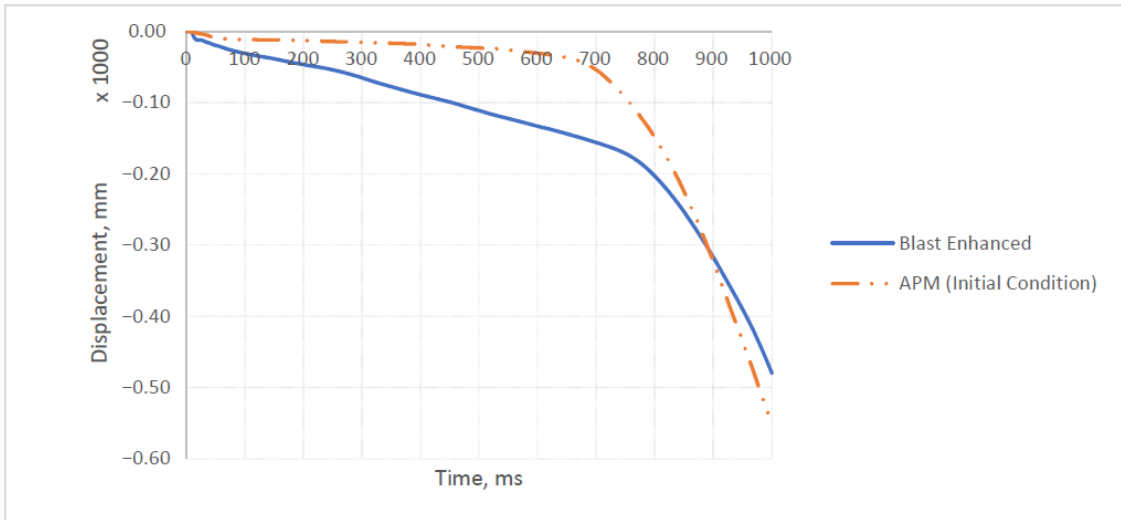


Figure 25. Nodal vertical displacement comparison at blast location 6.

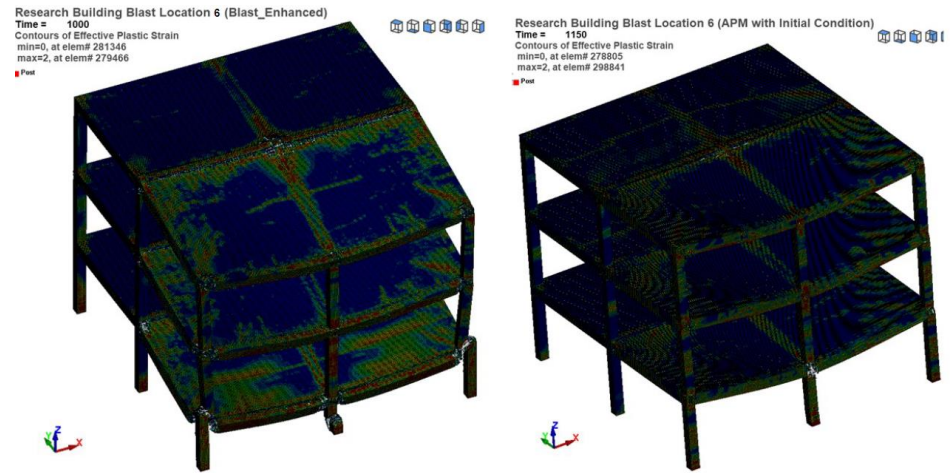


Figure 26. Blast_Enhanced and APM with the initial conditions method of analysis at partial collapse (blast location 6).

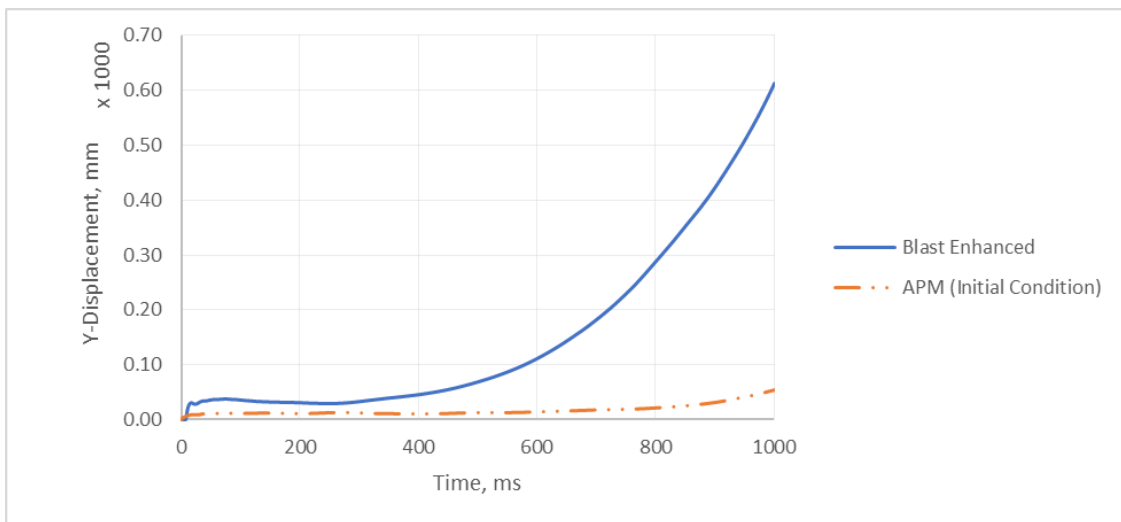


Figure 27. Nodal lateral displacement (Y-direction) comparison at blast location 6.

Similar to Figure 27, Figure 28 showed that the deviation in vertical velocity increased as time progressed. However, the rate of collapse followed a similar pattern after 650 ms.

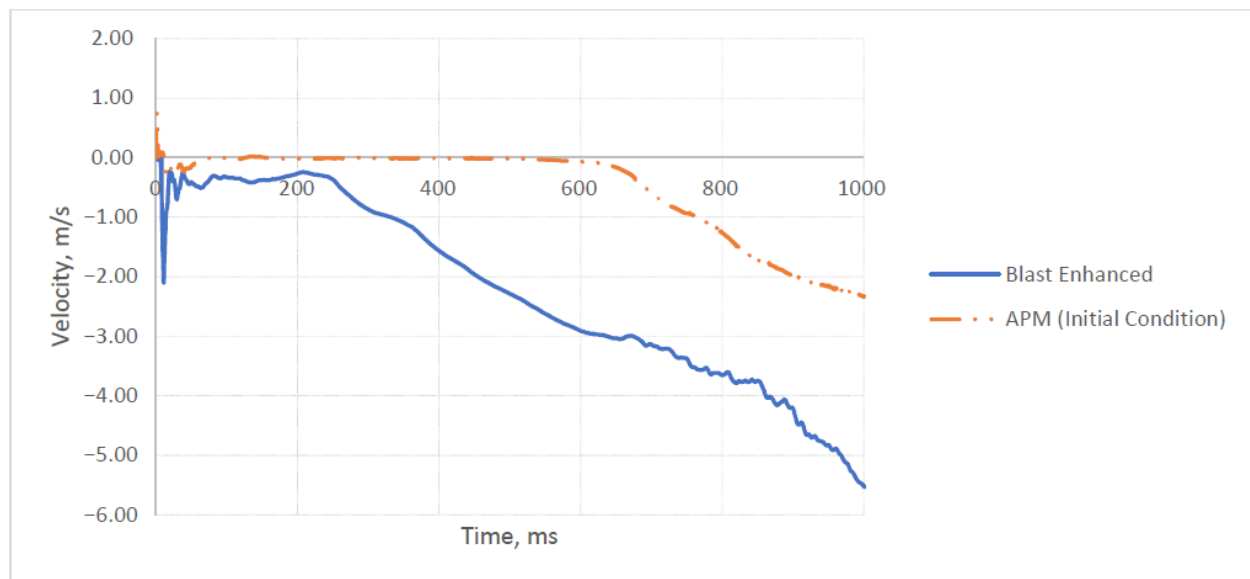


Figure 28. Nodal vertical velocity comparison at blast location 6.

This research investigated the overestimation of the APM method on the potential for progressive collapse and provided a method based on Shi et al. for accounting for the important parameters (initial conditions and damage) of the APM. The findings revealed that after a blast duration, columns were not in static equilibrium and sustained significant damage.

4. Conclusions

This research examined the accuracy of the Alternate Load Path Method (APM) in predicting progressive collapse under various blast scenarios. A representative building was initially designed for gravity and lateral loads, and 12 potential blast locations were selected for the study based on potential failure modes and access points. These locations were selected after several iterations to induce the failure of a single column at different blast locations. The variation in detonation height is intended to observe the different prevailing failure modes, flexure and direct shear. The blast load was determined using Kingery–Bulmash equations. Structural responses were evaluated using Single-Degree-of-Freedom (SDOF) analysis, considering high strain rates. Residual axial load capacity was calculated post-blast, incorporating concrete strain and rebar strength. The potential for progressive collapse was assessed via three methods: the APM, the APM with initial conditions, and benchmark blast–structure analysis.

1. The columns typically failed due to breach, flexure, or direct shear under blast loading, influenced by blast location and standoff distance. It is highly unlikely that columns fail in breach as the requirement for seismic demand usually leads to a higher column size. Direct shear failure is common in ground and close-in explosions, while flexural failure prevails in spherical blasts and at larger standoff distances.
2. The removal of critically damaged columns resulted in comparable responses between the APM with initial conditions and the benchmark analysis at blast locations 1 and 3, as well as between the APM and the benchmark analysis at blast location 3.
3. The APM with initial conditions provided reliable results at all blast locations but exhibited delays in collapse initiation and resulted in significant deviations in lateral displacement at blast location 6.

4. Based on these results, the following recommendations are proposed to explore the effects of blast waves in confined spaces and the use of ALE (Arbitrary Lagrangian-Eulerian) formulations in blast analysis.

Author Contributions: Conceptualization, B.M.; methodology, B.M.; software, B.M.; validation, B.M.; formal analysis, B.M.; investigation, B.M.; resources, B.M., B.H. and G.S.U.; data curation, B.M.; writing—original draft preparation, B.M.; writing—review and editing, B.M., B.H. and G.S.U.; visualization, B.M.; supervision, B.M., B.H. and G.S.U.; project administration, B.M., B.H. and G.S.U.; funding acquisition, B.M., B.H. and G.S.U. All authors have read and agreed to the published version of the manuscript.

Funding: This research received no external funding.

Institutional Review Board Statement: Not applicable.

Informed Consent Statement: Not applicable.

Data Availability Statement: The original data presented in the study are openly available from major research database such as Zenodo (<https://zenodo.org/>), accessed on 24 September 2024).

Conflicts of Interest: The authors declare no conflict of interest.

References

1. Department of Defense. *Design of Buildings to Resist Progressive Collapse*; Department of Defense: Washington, DC, USA, 2016.
2. LI, Z.; Shi, Y. Methods for progressive collapse analysis of building structures under blast and impact Loads. *Trans. Tianjin Univ.* **2008**, *14*, 329–339. [[CrossRef](#)]
3. Al-Salloum, Y.; Almusallam, T.; Ngo, T.; Elsanadedy, H.; Abbas, H.; Mendis, P. Progressive collapse analysis of medium-rise circular RC building against blast loads. In Proceedings of the ASME 2016 35th International Conference on Ocean, Offshore and Arctic Engineering, Busan, Republic of Korea, 19–24 June 19–24 2016.
4. Alshaikh, I.M.H.; Abadel, A.A.; Sennah, K.; Nehdi, M.L.; Tuladhar, R.; Alamri, M. Progressive collapse resistance of RC beam–slab substructures made with rubberized concrete. *Buildings* **2022**, *12*, 1724. [[CrossRef](#)]
5. Baker, W.E.; Cox, P.A.; Westine, P.; Kulesz, J.; Strehlow, R. *Explosive Hazards and Evaluation*; Elsevier: Amsterdam, The Netherlands, 1983.
6. de Carvalho, D.M.V.A. Simplified Analysis of RC Beam and Beam-Column Elements under Blast Loading. Master’s Thesis, Nova School of Science and Technology, NOVA University, Lisbon, Portugal, 2021.
7. Chiranjeevi, M.D.; Simon, J. Analysis of reinforced concrete 3D frame under blast loading and check for progressive collapse. *Indian J. Sci. Technol.* **2016**, *9*, 1–6. [[CrossRef](#)]
8. Galal, M.A.; Bandyopadhyay, M.; Banik, A.K. Progressive collapse analysis of three-dimensional steel–concrete composite building due to extreme blast load. *J. Perform. Constr. Facil.* **2020**, *34*, 14.
9. Siba, F. Near-Field Explosion Effects on Reinforced Concrete Columns: An Experimental Investigation. Master’s Thesis, Carleton University, Ottawa, ON, Canada, 2014.
10. Shi, Y.; Li, Z.-X.; Hao, H. A new method for progressive collapse analysis of RC frames under blast loading. *Eng. Struct.* **2010**, *32*, 1691–1703. [[CrossRef](#)]
11. Gombeda, J.M.; Naito, J.C.; Quiel, E.S.; Fallon, T.C. Blast-induced damage mapping framework for use in threat-dependent progressive collapse assessment of building frames. *Am. Soc. Civ. Eng.* **2016**, *31*, 04016089. [[CrossRef](#)]
12. Al-Salloum, Y.A.; Abbas, H.; Almusallam, T.H.; Ngo, T.; Mendis, P. Progressive collapse analysis of a typical RC high-rise tower. *J. King Saud Univ.—Eng. Sci.* **2017**, *29*, 313–320. [[CrossRef](#)]
13. Kassahun, A. *Blast Loading and Blast Effects on RC Frame Buildings*; Addis Ababa Institute of Technology: Addis Ababa, Ethiopia, 2011.
14. Department of Defense. *Unified Facilities Criteria—Structures to Resist the Effects of Accidental Explosions*; Department of Defense: Washington, DC, USA, 2008.
15. Munshi, J. State-of-the-art vs. State-of-the-practice in blast and progressive collapse design of reinforced concrete structures. In *Structures 2004: Building on the Past, Securing the Future, Proceedings of the 2004 Structures Congress, Nashville, Tennessee, 22–26 May 2004*; American Society of Civil Engineers: Reston, VA, USA, 2004; pp. 1–10.
16. Xu, J.X.; Liu, X.L. A two-step approach to progressive collapse analysis of building structures under blast loading. *J. Shanghai Jiaotong Univ. (Sci.)* **2009**, *14*, 393–397. [[CrossRef](#)]
17. McConnell, R.J.; Brown, H. Evaluation of progressive collapse alternate load path analyses in designing for blast resistance of steel columns. *Eng. Struct.* **2011**, *33*, 2899–2909. [[CrossRef](#)]
18. Jeyarajan, S.; Liew, J.Y.R.; Koh, C.G. Analysis of steel-concrete composite buildings for blast induced progressive collapse. *Int. J. Prot. Struct.* **2015**, *6*, 457–485. [[CrossRef](#)]

19. El-Shahat, F.M. Progressive Collapse Analysis of RC Building Frames with Different Seismic Design Levels. Master's Thesis, American University in Cairo, Cairo, Egypt, 2013.
20. EN 1990; Eurocode 0: Eurocode—Basis of Structural Design. CEN: Brussels, Belgium, 2002.
21. EN 1991-1-4; Eurocode 1: Actions on Structures—Part 1-4: General Actions—Wind Actions. CEN: Brussels, Belgium, 2005.
22. EN 1992-1-1; Eurocode 2: Design of Concrete Structures—Part 1-1 General Rules and Rules for Buildings. CEN: Brussels, Belgium, 2004.
23. EN 1998-1; Eurocode 8: Design of Structures for Earthquake Resistance—Part 1: General Rules, Seismic Actions and Rules for Buildings. CEN: Brussels, Belgium, 2004.
24. Cormie, D.; Mays, G.; Smith, P. (Eds.) *Blast Effects on Buildings*, 2nd ed.; Thomas Telford Publishing: London, UK, 2009.
25. Liu, Y.; Yan, J.; Li, Z.; Huang, F. Improved SDOF and numerical approach to study the dynamic response of reinforced concrete columns subjected to close-in blast loading. *Structures* **2019**, *22*, 341–365. [[CrossRef](#)]
26. General Services Administration. *Alternate Path Analysis & Design Guidelines for Progressive Collapse Resistance*; GSA Office of Design and Construction: Washington, DC, USA, 2016.
27. Yasseri, S. Iso-damage diagram for blast resistant design. *Res. Dev.* **2005**, *42*, 6–15.
28. Kyei, C. Effects of Blast Loading on Seismically Detailed Reinforced Concrete Columns. Master's Thesis, Carleton University, Ottawa, ON, Canada, 2014.
29. Krauthammer, T.; Bazeos, N.; Holmquist, T.J. Modified SDOF analysis of RC box-type structures. *J. Struct. Eng.* **1986**, *112*, 726–744. [[CrossRef](#)]
30. Cui, L.; Zhang, X.; Hao, H. Improved analysis method for structural members subjected to blast loads considering strain hardening and softening effects. *Adv. Struct. Eng.* **2021**, *24*, 2622–2636. [[CrossRef](#)]
31. Shi, Y.; Hao, H.; Li, Z.-X. Numerical derivation of pressure-impulse diagrams for prediction of RC column damage to blast loads. *Int. J. Impact Eng.* **2007**, *35*, 1213–1227. [[CrossRef](#)]
32. Warn, G.; Unal, G. *Estimating the Residual Axial Load Capacity of Flexure-Dominated Reinforced Concrete Bridge Columns*; Mid-Atlantic Universities Transportation Center: Charlottesville, VI, USA, 2014.
33. ACI 318-19; Building Code Requirements for Structural Concrete (ACI 318-19). American Concrete Institute: Farmington Hills, MI, USA, 2019.
34. U.S. Army Corps of Engineers. *User's Guide for the Single-Degree-of-Freedom Blast Effects Design Spreadsheets (SBEDS)*; U.S. Army Corps of Engineers: Omaha, NE, USA, 2008.
35. ASCE/SEI 59-22; Standard for Blast Protection of Buildings. ASCE: Reston, VA, USA, 2022.
36. Livermore Software Technology Corporation (LSTC). *LS-DYNA Keyword User's Manual Volume I*; Livermore Software Technology Corporation: Troy, MI, USA, 2021.
37. Zhang, D.; Yao, S.; Fangyun, L.; Chen, X.; Lin, G.; Wang, W.; Lin, Y. Experimental study on scaling of rc beams under close-in blast loading. *Eng. Fail. Anal.* **2013**, *33*, 497–504. [[CrossRef](#)]
38. Tantrapongsaton, W.; Hansapinyo, C.; Wongmatar, P.; Chaisomphob, T. Flexural reinforced concrete members with minimum reinforcement under low-velocity impact load. *Int. J. GEOMATE* **2018**, *14*, 129–136. [[CrossRef](#)]
39. Chopra, A.K. *Dynamics of Structures Theory and Applications to Earthquake Engineering*; Pearson Education Limited: Harlow, UK, 2020.
40. Timsah, Y.; Khatib, A.; Jahami, M.K.; Sonebi, M. Numerical analysis of a reinforced concrete beam under blast loading. In *MATEC Web of Conferences, Proceedings of 2nd International Congress on Materials & Structural Stability (CMSS-2017), Rabat, Morocco, 22–25 November 2017*; EDP Sciences: Les Ulis, France, 2018; Volume 149, p. 02063.
41. Abebe, S.D.; Alemu, T.M.; Urgessa, G. Progressive collapse of typical and atypical reinforced concrete framed buildings. *Int. J. Concr. Struct. Mater.* **2024**, *18*, 36.

Disclaimer/Publisher's Note: The statements, opinions and data contained in all publications are solely those of the individual author(s) and contributor(s) and not of MDPI and/or the editor(s). MDPI and/or the editor(s) disclaim responsibility for any injury to people or property resulting from any ideas, methods, instructions or products referred to in the content.